# Electrostatic modulation of multiple binding events between loquacious-PD and double-

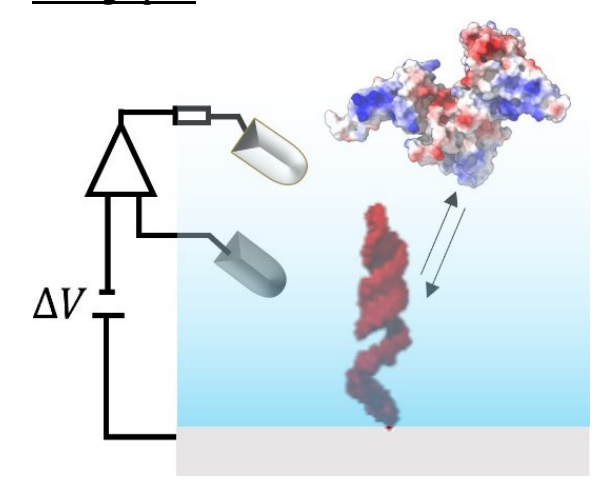
# stranded RNA

Sasha A. Moonitz,<sup>a</sup> Nhat T. Do <sup>a</sup> and Rodrigo Noriega \*<sup>a</sup>

<sup>a</sup> Department of Chemistry, University of Utah, Salt Lake City Utah 84112

\* Contact: noriega@chem.utah.edu

### TOC graphic



# **ABSTRACT**

Electrostatics can alter the RNA-binding properties of proteins that display structure selectivity without sequence specificity. Loquacious-PD relies on this broad scope response to mediate the interaction of endonucleases with double stranded RNAs. Multimodal spectroscopic probes with *in situ* perturbations reveal an efficient and stable binding mechanism that disfavors high protein density complexes and is sensitive to local electrostatics.

#### INTRODUCTION

RNA-binding proteins (RBPs) are a critical component in the production, translation, localization, and degradation of RNA.<sup>1</sup> A diverse class of proteins,<sup>2</sup> RBPs bind their targets with varying degrees of sequence, structure, and context specificity,<sup>3</sup> and their molecular recognition properties rely on a complex set of interactions.<sup>4</sup> Electrostatic forces and dynamic conformations are important for protein-RNA binding,<sup>5</sup> but assessing their role in substrate recruitment and complex stability is challenging, especially when multiple protein domains are involved.

Studies of protein-RNA interactions rely on a variety of tools to measure structural, kinetic, and thermodynamic properties. However, currently available methods are rarely capable of introducing controlled *in situ* perturbations to the environment in which binding takes place, and vast differences in sample conditions can hinder the comparability of results across techniques. Interrogating the binding mechanism of complex biomolecules from a molecular perspective that accounts for their local environment requires a multi-pronged approach. One way to achieve these goals is to combine time-resolved fluorescence and surface plasmon resonance measurements on functionalized transparent

electrodes,<sup>8</sup> a multimodal approach that incorporates distinct observables to yield complementary information while introducing a controllable local electrostatic perturbation to the interactions between binding partners – vs. bulk perturbations to dielectric screening.<sup>9</sup> Importantly, a bifunctional silane self-assembled monolayer localizes the formation of biomolecular complexes to an electrified interface with generalizable surface functionalization protocols.<sup>10</sup> Combining plasmonic and fluorescence-based readouts enables complementary measurements of equilibrium dissociation constants, dielectric properties at the interface and bulk (e.g., surface coverage, refractive index), as well as association and dissociation rates. This versatile platform for probing protein-RNA binding under the effect of an interfacial electric field is valuable because electrostatic forces are prevalent in biomolecular interactions, and disrupting those interactions provides an approach to quantify their relevance in complex formation and stability.

The binding of double-stranded RNA (dsRNA) by loquacious-PD (Loqs-PD) is an interesting model to probe electrostatic effects in protein-RNA interactions. Loqs-PD is essential for the efficient biogenesis of endogenous siRNAs in *D. melanogaster*,<sup>13</sup> assisting the endonuclease Dicer-2's recruitment of suboptimal dsRNA substrates.<sup>11</sup> With two dsRNA binding motifs (dsRBMs), Loqs-PD recognizes a wide range of targets, binding anywhere along a dsRNA strand (**Fig. 1**).<sup>11f</sup> Multiple protein copies can bind to one dsRNA, but cooperativity has not been reported.<sup>11a</sup> Importantly, the mode in which multiple Loqs-PD copies bind a single dsRNA and the effect of local electrostatics on complexes with different stoichiometries is unexplored. Here, we measured the binding of dsRNA by Loqs-PD at an electrified interface using plasmonic and fluorescence probes. Kinetic measurements revealed an efficient initial binding step, and stoichiometry-dependent dissociation constants suggest high protein density is disfavored. The formation and stability of these protein:RNA complexes is altered by local electrostatics in a stoichiometry-dependent manner.

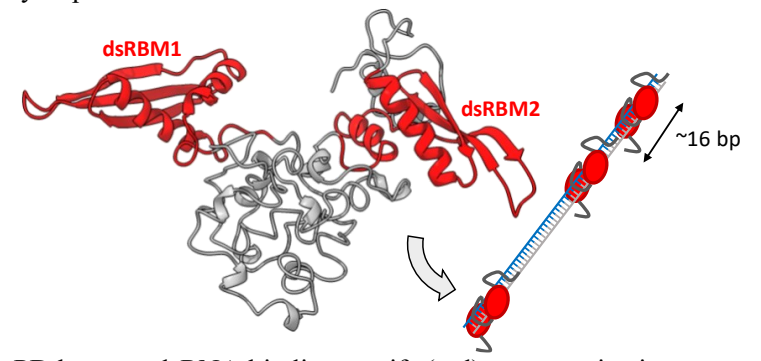


**Figure 1.** Loqs-PD has two dsRNA binding motifs (red) to recognize its targets, and a binding footprint of ~16 base pairs on the dsRNA strand. <sup>11a</sup> Protein structure predicted with trRosetta <sup>12</sup> and equilibrated with molecular dynamics simulations (**Fig. S1**).

#### **RESULTS and DISCUSSION**

Surface plasmons are electromagnetic waves formed when the transverse wavevector of light incident at a conductor/dielectric boundary couples resonantly to charge oscillations on the conductor's surface. <sup>14</sup> Because the strength and incidence angle response of surface plasmon resonances (SPR) depend on the dielectric properties at this interface, they provide a sensitive probe of ligand recognition for surface-immobilized targets. <sup>14</sup> Typical SPR sensors employ noble metals with resonances in the visible spectrum,

but their broadband optical response and propensity to quench excited states prevents their integration with other light-based stimuli. An alternative is to use doped wide bandgap metal oxides (e.g. indium tin oxide, ITO) with plasmon resonances in the mid-infrared.<sup>8,15</sup>

64

65

66

67

68

69

70 71

72

73

74

75

76

77 78

79 80

81

82

83

84

85

86

87

88

89

90

We measured the reflectance of a 2550 nm laser beam directed to the SPR sensor chip through a coupling prism (Kretschmann configuration) as a function of rotation angle before and after the addition of buffer to the sample chamber. A transfer matrix model of these SPR resonances (Fig. S2, Table S1) was used to determine their free carrier density ( $\langle N_e \rangle = 4.6 \pm 0.7 \times 10^{20} \, \mathrm{cm}^{-3}$ ), thickness ( $\langle h_{ITO} \rangle = 235 \pm 0.7 \times 10^{20} \, \mathrm{cm}^{-3}$ ) 16 nm), and sensitivity ( $\langle \partial R / \partial n \rangle = 6.3 \pm 1.4$ ). Once each sensor's response was recorded, it was positioned at an angle at the midpoint of the sharp dip in reflectance (the SPR sensing angle,  $\theta_s$ ), RNA targets were attached in situ (details in ESI, Fig. S3), and the reflectance of the infrared laser beam was monitored as a function of Loqs-PD concentration over a series of additions of protein aliquots. Loqs-PD:dsRNA complexes at the sensor's surface increase the local refractive index and shift the SPR resonance to shallower angles, increasing the reflectance measured at  $\theta_s$  (Fig. 2). This binding response was expected to follow a Langmuir isotherm, 16 reaching saturation once all binding sites are occupied. However, due to the substantial penetration depth of mid-IR plasmon evanescent waves ( $\delta_{SPR}^{IR} \sim 1.2 \, \mu \text{m}$ vs  $\delta_{SPR}^{vis} \sim 180$  nm), 14 changes in the bulk refractive index led to a linear response at high protein concentrations (Fig. S5) – an onboard calibration used to estimate the concentration of Logs-PD bound to the surface-anchored RNA. Dissociation constants  $(K_D)$ , saturation amplitudes of binding response (A), and chip responsivities  $(\partial R / \partial c)$  were obtained by nonlinear fitting (**Table S2**).

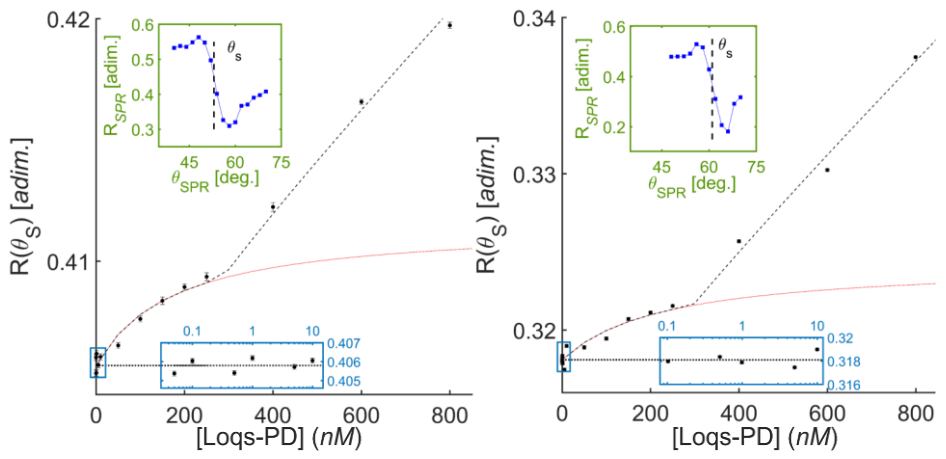
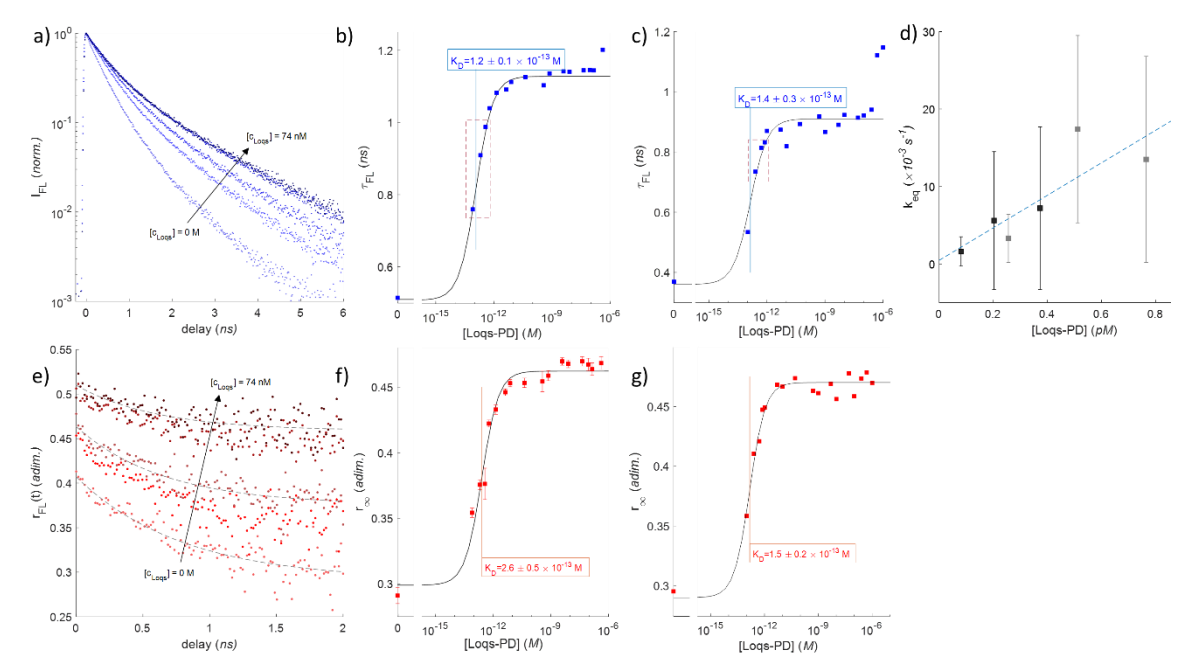


Figure 2. The reflectance of a mid-IR laser coupled to the surface plasmon resonance of ITO electrodes increases as protein is added to the sample chamber, both under open circuit conditions (left) and with an electric bias (500 mV vs. Ag/AgCl, right). Markers indicate measured reflectance, averaged over 5 mins.; error bars are  $\pm$  one standard error of the mean. Dotted horizontal line denotes the reflectance starting value  $R_0$ . Signal was described by a binding isotherm (red line) plus a linear response (combined fit as dashed black lines). Upper insets depict the plasmon resonance for each sensor in blank buffer (blue squares), with the sensing angle  $\theta_s$  shown. Lower insets show signal at lowest protein concentrations. Additional SPR responses in ESI (Fig. S4).

91 In open circuit conditions, we measured an average dissociation constant for Loqs-PD:dsRNA complexes of  $K_D^{oc} = 120 \pm 50$  nM, in line with values reported using steady state fluorescence anisotropy (62 nM) 92 and gel mobility shift assays (9 nM). 11a,f The surface coverage of Loqs-PD at saturation,  $\Gamma_{prot} \approx$ 93 94  $2.2 \times 10^{10}$  cm<sup>-2</sup>, is comparable to the surface coverage of RNA measured with ex situ elemental analysis  $(\Gamma_{RNA} \sim 10^{10} \text{ cm}^{-2}, \text{ Fig. S6} \text{ and Table S3})$ . The responsivity of the SPR chip measured in binding 95 experiments  $(\partial R / \partial c)$  together with the sensitivity extracted from models of the full SPR curve  $(\partial R / \partial c)$ 96 97  $\partial n$ ) can estimate the change in refractive index as a function of protein concentration at mid-IR 98 wavelengths, with an average value of  $\langle \partial n / \partial c \rangle \sim 0.06$  mL/mg that compares well to values reported for a wide variety of protein solutions at visible and near-IR wavelengths.<sup>17</sup> When a positive bias of 500 99 100 mV (vs. Ag/AgCl) was applied, the dissociation constant increased to  $K_D^{+\Delta V} = 280 \pm 130$  nM, but the 101 protein coverage at saturation did not change. This weakened interaction was expected since an electric 102 field directed away from the ITO and into the buffer perturbs the binding between Logs-PD's positively-103 charged dsRBMs and the negatively-charged nucleic acid. 104 By detecting changes in the refractive index at the sensing interface due to complex formation, mid-IR 105 plasmons indicate that the molecular recognition properties of Loqs-PD are sensitive to electrostatic 106 perturbations. For a complementary view of this binding process - as sensed by the surface-tethered 107 binding partner - we performed time-resolved fluorescence experiments of fluorescent probes attached 108 to the distal terminus of surface-anchored dsRNA targets. 109 The polarization-resolved ultrafast fluorescence of fluorophore-labeled dsRNA anchored to ITO was used 110 to report on changes to the photophysics of the fluorescent probe (Cy3) due to protein binding. In the 111 same liquid cell used for mid-IR SPR experiments (but without the coupling prism), the fluorescence 112 from RNA-functionalized ITO coverslips was measured first for dry samples, then after adding buffer, applying a voltage (if used), and during sequential additions of protein aliquots. As observed in binding 113 studies of dsRNA, Loqs-PD, and Dicer-2 performed in bulk solution, 11c rigidifying the local environment 114 115 of Cy3 labels lengthens their fluorescence lifetime and increases their residual transient fluorescence 116 anisotropy. Multichannel time-tagged time-resolved photon detection yields kinetic traces for the 117 fluorescence lifetime of chromophores labeling surface-anchored dsRNA and their time-averaged (equilibrium) fluorescence lifetime and fluorescence anisotropy decays. 118



**Figure 3.** The fluorescence decay (a) and transient fluorescence anisotropy (e) of Cy3 chromophores labeling dsRNA anchored to ITO supports reveal changes in their photophysics due to binding by Loqs-PD. These changes in the fluorescence lifetime (b,c) and residual anisotropy (f,g) are well-described by Langmuir isotherms. Equilibration rates as a function of concentration (d, black and gray markers are data from points inside dashed rectangle in c and d, respectively) support these observations and provide information on the association and dissociation rates for this binding event (details in ESI).

In open circuit, binding of surface-tethered Cy3-dsRNA by Loqs-PD lengthens the fluorescence lifetime of Cy3 labels (**Fig. 3a**) and hinders the relaxation of their fluorescence anisotropy (**Fig. 3e**). Notably, these changes in the photophysics of dye-labeled dsRNA take place at considerably lower protein concentrations than those which resulted in a measurable mid-IR SPR response. Fitting Langmuir isotherms to time-averaged fluorescence lifetime (**Fig. 3b,c**) and residual anisotropy (**Fig. 3f,g**) of surface-anchored Cy3-dsRNA as a function of Loqs-PD concentration reveals a sub-pM dissociation constant—with an average  $K_D^{oc} = 1.7 \pm 0.2 \times 10^{-13}$  M. If a kinetic trace was observed (dashed rectangles in **Fig. 3b,c**), its equilibration rate  $k_{eq}$  was computed by fitting an exponential relaxation between the starting and final values ( $k_{eq}$  values in **Fig. 3d** and **Table S4**, kinetic traces and fits in **Fig. S7**). These kinetics are dictated by association and dissociation rates ( $k_{eq} = k_{on} \cdot c_{Loqs} + k_{off}$ ,  $k_{on} \approx 2 \times 10^{10}$  M<sup>-1</sup>s<sup>-1</sup>,  $k_{off} \approx 4 \times 10^{-4}$  s<sup>-1</sup>) consistent with  $K_D^{oc}$  from Langmuir isotherms and suggest diffusion-limited binding.

At protein concentrations  $c_{Loqs} > 150$  nM, an additional change in the time-averaged fluorescence lifetime of Cy3-dsRNA substrates can be observed (**Fig. 3b,c**); however, this signal is not as robust as that in the photophysical changes at lower protein concentrations. Interestingly, this response is in line with that measured in mid-IR SPR sensors. Kinetic traces (**Fig. S7**) measured at these higher concentrations suggest that, compared to the rates calculated for the earlier binding event, these

complexes form with a significantly lower association rate  $(k'_{on} \sim 10^3 \text{ M}^{-1} \text{s}^{-1})$  but no discernible change to their dissociation rate  $(k'_{off} \sim 10^{-4} \text{ s}^{-1})$ .

143

144

145146

147

148149

150

151152

153

154

155

156

157

158

159

160161

162

163

164

165

166

167

168

169

170

171

172

173

174

175

The application of a voltage to the ITO electrode (500 mV vs. Ag/AgCl) alters the conformation of dsRNA on the sensor surface and their binding by Loqs-PD. Prior to adding Loqs-PD, a positive bias to the ITO electrode leads to longer fluorescence lifetimes and larger residual anisotropies for surface-anchored Cy3dsRNA. These observations can be explained by noting that nucleic acids are negatively-charged polyelectrolytes whose conformation atop electrodes can be modified with an external bias – as seen in fluorescence quenching assays of DNA on Au electrodes. 18 The dsRNA employed in this work are shorter than their persistence length<sup>19</sup> and are anchored with a flexible linker, so it is likely that the dsRNA is attracted toward the electrode without substantial bending - although mechanical stress can distort their minor groove and affect their binding by dsRBMs.<sup>20</sup> This change in the initial conditions upon which Loqs-PD binds dsRNA alters their complex formation (Fig. 4). In these conditions, the average fluorescence lifetime of Cy3-dsRNA is shortened upon binding, and its residual anisotropy is reduced (or at most, it does not increase as noticeably as with complexes formed in open circuit conditions). Fitting a Langmuir binding isotherm to this decrease in fluorescence lifetime upon addition of Loqs-PD yields an average dissociation constant  $K_D^{+\Delta V}=4.5\pm2.6$  pM. A voltage-dependent reduction in fluorescence signal is responsible for the observed variability in time-resolved fluorescence data. Such reduction is not specific to the Cy3 labeled dsRNA in this work; it has also been observed in fluorescein-labeled polypeptide films.<sup>8,21</sup> The source of this brightness reduction does not appear to be an increase in nonradiative decay rates; such quenching would be accompanied by a shortened fluorescence lifetime with voltage, which is not observed. This electric fielddependent decrease in fluorescence output is a topic of current study in our group, and it may be caused by a detuning of electronic transitions at an electrified interface, or by a preferential alignment of chromophores near the interface that reduces the overlap between their transition dipole moment and the laser polarization. This reduction in brightness has a larger effect on the anisotropy traces, due to their calculation as the relative difference between orthogonal polarization channels whose fluctuations become important at lower photon counts. Thus, trends in residual anisotropy contain a larger amount of scatter and are best described qualitatively (Langmuir binding curves yield K<sub>D</sub>~10 pM but with considerable uncertainty). Nevertheless, clear differences in Loqs-PD:dsRNA binding are observed as a function of the local electrostatic conditions in which molecular recognition takes place (primarily in the fluorescence lifetime measurements, Fig. 4a). As was the case for mid-IR SPR experiments, a positive bias to the RNA-functionalized electrode weakens their binding by protein in solution; however, the relative change is larger in the high-affinity binding event monitored by fluorescence  $(K_D^{+\Delta V}/K_D^{oc} \sim 25)$  than for lower-affinity complex formation measured with mid-IR plasmonics  $(K_D^{+\Delta V}/K_D^{oc} \sim 2)$ .

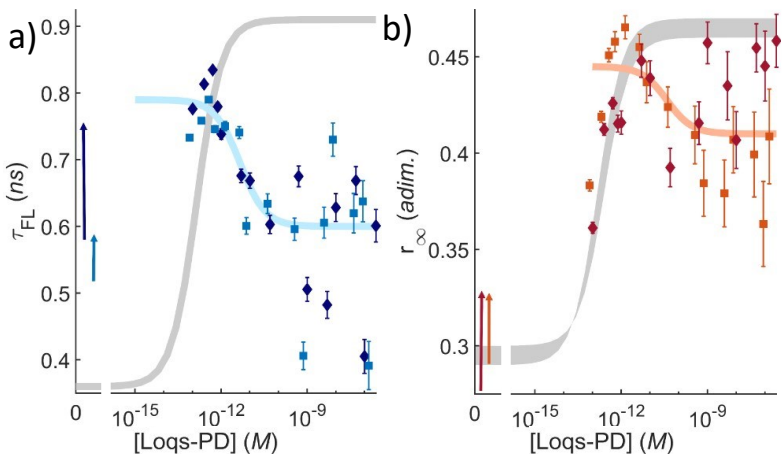


**Figure 4.** When atop a biased ITO electrode (+500 mV vs Ag/AgCl), binding by Loqs-PD leads to a distinct trend in the fluorescence lifetime (a) and residual fluorescence anisotropy (b) of Cy3-dsRNA. Independent trials as light/dark markers, shaded blue/orange curves are Langmuir isotherms with parameters averaged over trials. Vertical arrows show observed changes in the photophysics of samples in buffer upon voltage application. Average behavior in open circuit conditions shown for comparison (gray shades).

176

177

178

179

180

181

182

183

184 185

186

187

188

189

190 191

192193

194

195

196

197

198199

200

201

202

203

Before further discussing electrostatic perturbations, it is valuable to combine our multimodal observations in open circuit conditions to construct a model for Loqs-PD:dsRNA complex formation. Loqs-PD has two dsRBMs that can bind independently and it is possible for multiple copies of Loqs-PD to bind along a single dsRNA – with a footprint of ~16 base pairs per protein copy. 11a,f For our 52-nt long dsRNA substrates, one could envision two possibilities: (1) partial vs. complete binding of one protein copy, or (2) binding of one vs. two protein copies. The latter is more consistent with our data. The fluorophore attached to dsRNA responds to changes in its local environment so it should be mostly sensitive to initial complex formation; subsequent protein binding is expected to have a smaller effect on its photophysics. As complexes with increasing stoichiometry are formed, protein would continue to accumulate at the interface, which would explain why mid-IR SPR sensors are sensitive to the second event but not to the first. Interestingly, additive binding of two dsRBMs with  $K_D^{dsRBM} \sim 200$  nM separated by a 45-aa linker predicts a sub-pM affinity, 11f,22 and single copies of Loqs-PD can bind at sub-nM concentrations. 11a Thus, we interpret our data as the sequential binding of Logs-PD to dsRNA. Initially, 1:1 complexes form with an equilibrium dissociation constant  $K_D \sim 10^{-13} \,\mathrm{M}$  and association and dissociation rates  $k_{on} \sim 10^{10} \text{ M}^{-1} \text{s}^{-1}$ ,  $k_{off} \sim 10^{-4} \text{s}^{-1}$ ; binding of an additional copy of Loqs-PD leads to a 2:1 complex with equilibrium dissociation constant  $K_D' \sim 10^{-7}$  M and association and dissociation rates  $k'_{on} \sim 10^3 \text{ M}^{-1} \text{s}^{-1}, k'_{off} \sim 10^{-4} \text{ s}^{-1}.$ 

An external bias at the interface where Loqs-PD:dsRNA complex formation takes place affects their binding. Most noticeably, the dissociation constants for both the higher- and lower-affinity binding events display a measurable increase. Lower signal and longer integration times prevented the determination of whether this bias dependence in dissociation constants was due to changes in the association or dissociation of Loqs-PD:dsRNA complexes — or both. Moreover, an applied voltage alters the

conformation of dsRNA anchored to an electrode and is a likely contributor to observed differences in binding. Nevertheless, these results confirm the important role of electrostatics in the molecular recognition properties of Loqs-PD toward dsRNA.

206 207 208

209

210

211

212

213

214

215

216

217

218

219 220

221

222

223

224

225

226 227

228

229

230 231

232

233

234

235

236

237

238

239

240

241 242

204

205

# **CONCLUSION**

In summary, multimodal observations with controllable in situ perturbations revealed valuable insights on the biomolecular interactions that underpin the function of Loqs-PD. First, the fast association rate for 1:1 Loqs-PD:dsRNA complexes suggests a binding mechanism in the diffusion-limited regime.<sup>23</sup> Second, the weaker interaction in 2:1 complexes implies that high protein density binding is disfavored – our dsRNA substrates (52-nt) are short compared to the Loqs-PD binding footprint (~16 bp), so 2:1 complexes must accommodate protein copies in close proximity. And third, the modulation of binding by an electrical bias underscores the role of electrostatics on the formation and stability of these complexes – a key factor in a molecular recognition mechanism that is selective for nucleic acid structure without being specific to their sequence. This work examined the RNA-binding protein loquacious-PD – an essential component in the production of endogenous siRNA in D. melanogaster. We report the electrostatic modulation of the formation of Logs-PD:dsRNA complexes with stoichiometry-dependent association rates and dissociation constants. To determine the role of electrostatic interactions on this binding process, we employed steady-state and kinetic experiments that combine mid-infrared plasmonics and time-resolved visible fluorescence with an in situ electrostatic perturbation of the binding environment. In this way, we found that the initial binding of Loqs-PD to dsRNA is a high-affinity interaction ( $K_D \sim 10^{-13}$  M) with a diffusion-limited association rate  $(k_{on} \sim 10^{10} \text{ M}^{-1} \text{s}^{-1})$ , and that the formation of 1:1 Loqs-PD:dsRNA complexes is sensitive to electrostatic perturbations  $(K_D^{+\Delta V}/K_D^{oc} \sim 25)$  – with a mechanism that likely involves changes to dsRNA conformation at an electrified interface. Binding of an additional protein copy yields 2:1 complexes that, in comparison to 1:1 complexes, display a substantially weaker interaction ( $K_D' \sim 10^{-7}$  M) due to a slower association rate  $(k'_{on} \sim 10^3 \,\mathrm{M}^{-1} \mathrm{s}^{-1})$  but similar dissociation rate, and a reduced but still significant sensitivity to electrostatic perturbations  $(K_D^{\prime+\Delta V}/K_D^{\prime oc} \sim 2)$ . These observations support a model for the dsRNA recognition properties of Logs-PD in which initial binding is efficient and stable, the formation of complexes with high protein density is disfavored, substrate conformation plays a substantial role, and electrostatics are important. It is valuable to consider these molecular recognition properties of Loqs-PD in the context of its biochemical function. A fast association rate coupled with a susceptibility to structural and electrostatic perturbations allow it to effectively bind a broad scope of dsRNA targets with varied sequences, and its low tendency to bind at high density on the same dsRNA strand may be connected to its ability to independently interact with either of its partners (dsRNA and Dicer-2) in order to form a functional dsRNA:Loqs-PD:Dicer-2 complex for siRNA production. A fundamental description of molecular recognition in nucleic acid binding proteins must include

controlled studies of the effects of local electrostatics - whose key role has been recently highlighted by the acceleration in target search due to intramolecular electrostatic interactions. <sup>24a</sup> Together with new biophysical tools - such as advanced NMR techniques to map electrostatic potentials on the surface of biomolecules,<sup>24b</sup> and high-resolution determination of complex structures – our approach will contribute to the understanding of ubiquitous electrostatic interactions in protein-nucleic acid and protein-protein complexes. In this work, we employed a well-defined *in vitro* environment as a means to introduce a controllable electrostatic perturbation, which opens the door to studies of electrostatic interactions relevant to *in vivo* situations including protein-RNA binding at highly charged locations such as ribosomal complexes (for nascent RNAs) and the nuclear envelope (for nucleic acid translocation), and can serve as a platform to test the functional importance of electrostatic charge at biologically relevant interfaces such as cytoplasmic membranes and viral envelopes. Most importantly, this methodology is readily compatible with dynamic perturbations (e.g., optically-gated pH gradients) as well as with the combination of multiple stimuli,<sup>21</sup> offering unique opportunities to control the forces that mediate the interactions between biological macromolecules.

254255

243244

245

246

247

248

249

250

251

252253

#### **ACKNOWLEDGMENTS**

- We gratefully acknowledge funding by the U.S. National Science Foundation (NSF MCB-2123516) and
- resources from the Center for High Performance Computing and the Micron Technology Foundation Inc.
- 258 *Microscopy Suite* at Univ. of Utah (Kratos XPS acquired with support from NSF CHE-0443657).

259260

#### **Conflicts of interest**

There are no conflicts to declare.

262

263

#### REFERENCES

- [a] MJ Moore. Science 2005, 309, 1514 [b] DD Licatalosi, RB Darnell. Nat Rev Genet 2010, 11, 75 [c] E Holmqvist,
   J Vogel. Nat Rev Microbiol 2018, 16, 601.
- [a] MW Hentze, A Castello, T Schwarzl, T Preiss. *Nat Rev Mol Cell Biol* 2018, *19*, 327 [b] GR Gronland, A Ramos.
   Biochem Soc Trans 2017, *45*, 1305 [c] D Ray et al. *Nature* 2013, *499*, 172
- 3 [a] E Jankowsky, ME Harris. *Nat Rev Mol Cell Biol* 2015, *16*, 533. [b] AR Ferré-D'Amaré,. *Cell Chem Biol* 2016,
  269 23, 1177. [c] D Dominguez, P Freese, M.S. Alexis, A. Su, M. Hochman, T. Palden, C Bazile, NJ Lambert, EL Van
  Nostrand, GA Pratt, GW Yeo, BR Graveley, CB Burge. *Mol Cell* 2018, *70*, 854.
- 271 4 M Corley, MC Burns, GW Yeo. *Mol Cell* 2020, 78, 9.
- 5 [a] S Shazman, Y Mandel-Gutfreund. *PLOS Comp Biol* 2008, 4, e1000146. [b] YC Chen, C Lim. *Nuc Ac Res* 2008,
   36, e29. [c] S Jones, DT Daley, NM Luscombe, HM Berman, JM Thornton. *Nuc Ac Res* 2001, 29, 943. [d] DD Boehr,
   R Nussinov, PE Wright. *Nat Chem Biol* 2009, 5, 789.
- 275 6 L Dimitrova-Paternoga, PKA Jagtap, P-C Chen, J Hennig. Structure 2020, 28, 6
- 276 7 R Noriega. J. Phys. Chem. B 2021, 125, 5667
- 8 SA Moonitz, N Shepard, R Noriega. J Mat Chem B 2020, 8, 7024
- [a] TB Updegrove, JJ Correia, Y Chen, C Terry, RM Wartell. RNA 2011, 17, 489. [b] E Seyrek, PL Dubin, C Tribet,
   EA Gamble. Biomacromol 2003, 4, 273. [c] K Ariga, EV Anslyn. J Org Chem 1992, 57, 417. [d] SS Athavale, W
   Ouyang, MP McPike, BS Hudson, PN Borer. Biochem 2010, 49, 3525. [e] JJ McDermott, B Civic, A Barkan. PLOS
- 281 *ONE* 2018, *13*, e0209713.
- [a] A Kumar, O Larsson, D Parodi, Z Liang. *Nuc Ac Res* 2000, 28, e71. [b] B Joos, H Kuster, R Cone. *Anal Biochem* 1997, 247, 96. [c] Z Guo, RA Guilfoyle, AJ Thiel, R Wang, LM Smith. *Nuc Ac Res* 1994, 22, 5456.

- 284 11 [a] KD Trettin, NK Sinha, DM Eckert, SE Apple, BL Bass. PNAS 2017, 114, E7939. [b] NK Sinha, KD Trettin, PJ
- Aruscavage, BL Bass. Mol Cell 2015, 58, 406 [c] M Jonely, RK Singh, HM Donelick, BL Bass, R Noriega Chem.
- 286 Commun. 2021, 57, 10879. [d] S Su, J Wang, T Deng, X Yuan, J He, N Liu, X Li, Y Huang, H-W Wang, J Ma.
- 287 Nature 2022, 607, 399. [e] M Naganuma, H Tadakuma, Y Tomari. Nat Commun 2021, 12, 4268. [f] J-N Tants, S
- Fesser, T Kern, R Stehle, A Geerlof, C Wunderlich, M Juen, C Hartlmüller, R Böttcher, S Kunzelmann, O Lange, C
- Kreutz, K Förstemann, M Sattler. Nuc Ac Res 2017, 45, 12536.
- 290 12 Z Du, H Su, W Wang, L Ye, H Wei, Z Peng, I Anishchencko, D Baker, J Yang. Nat Prot 2021, 16, 5634.
- 291 13 R Zhou, B Czech, J Brennecke, R Sachidanandam, JA Wohlschlegel, N Perrimon, GJ Hannon. RNA 2009, 15, 1886.
- 292 14 J Dostálek, CJ Huang, W Knoll, in Surface Design: Applications in Bioscience and Nanotechnology, eds. R Forch,
- H Schonherr, ATA Jenkins, Wiley-VCH, Weinheim, 2009, 29.
- 15 C Rhodes, S Franzen, J-P Maria, M Losego, DN Leonard, B Laughlin, G Duscher, S Weibel. *J App Phys* 2006, *100*,
   054905.
- 296 16 H Swenson, NP Stadie. *Langmuir* 2019, *35*, 5409.
- 17 [a] D Khago, JC Bierma, KW Roskamp, N Kozlyuk, RW Martin. *J Phys Cond Matt* 2018, *30*, 435101. [b] H Zhao,
   PH Brown, P Schuck. *Biophys J* 2011, *100*, 2309
- 299 18 PS Spuhler, J Knežević, A Yalçin, Q Bao, E Pringsheim, P Dröge, U Rant, MS Ünlü. PNAS 2010, 107, 1397.
- 300 19 [a] JA Abels, F Moreno-Herrero, T van der Heijden, C Dekker, NH Dekker. *Biophys J* 2005, 88, 2737. [b] P 301 Kebbekus, DE Draper, P Hagerman. *Biochem* 1995, 34, 4354.
- 20 [a] BM Lunde, C Moore, G Varani. Nat Rev Mol Cell Biol 2007, 8, 479. [b] A Marin-Gonzalez, JG Vilhena, R Perez,
   F. Moreno-Herrero. PNAS 2017, 114, 7049.
- 304 21 SA Moonitz, R Noriega. Macromol Rapid Commun 2023, 44, 2200635.
- 305 22 Y Shamoo, N Abdul-Manan, KR Williams. Nuc Ac Res 1995, 23, 725
- 306 23 KR Gleitsman, RN Sengupta, D Herschlag. RNA 2017, 23, 1745.
- 307 24 [a] X Wang, LS Bigman, HM Greenblatt, B Yu, Y Levy, J Iwahara. *Nuc Ac Res* 2023, *51*, 4701. [b] B Yu, CC Pletka,
   308 BM Pettitt, J Iwahara. *PNAS* 2021, *118*, e2104020118.